Full-field Characterisation of a Fatigue Crack – Crack Closure Revisited

J. Tong[1*], S. Alshammrei[1], T. Wigger[1], C. lupton[1], J. R. Yates[2]
[1]University of Portsmouth, UK
[2]SIMULINE Ltd, UK
* jie.tong@port.ac.uk

ABSTRACT

The full fields of a fatigue crack tip, ahead and behind the crack tip, have examined in this work using Digital Image Correlation (DIC). We measured, *in situ,* the surface crack opening displacement (COD) at selected locations behind the crack tip and the evolution of the near-tip displacements and strains ahead of the crack tip during loading and unloading in a model material, stainless steel 316L, of a standard compact tension (CT) specimen. In addition, the stress intensity factor for the CT specimen was also estimated from the Williams' series expansion using the displacements obtained from DIC as a function of applied load. The results present a complete picture of the crack tip field at the selected load levels, where events both ahead and behind of the crack tip were studied for the first time in terms of crack driving and attenuation effects.

We hope the results provide some fundamental insights into the full-field behaviour of a crack tip under cyclic loading conditions; and shed light on the phenomenon of crack closure and its relevance to the fatigue crack driving force ΔK under small scale yielding conditions.

KEYWORDS: Crack closure; crack tip; DIC; fatigue crack growth; strain; stress intensity factor

INTRODUCTION

Characterisation of fatigue crack growth has been of great interest in damage tolerance assessments of fracture-critical engineering components and structures. It has been generally accepted that the use of an elastic stress intensity factor range, ΔK, is adequate in most of the engineering applications under small scale yielding (SSY) conditions. Paris *et al*[1] were the first to use the stress intensity factor range to correlate fatigue crack growth rates obtained from three independent studies. Rice[2] further rationalised this approach within the framework of continuum mechanics, and suggested that fatigue crack growth rate data can be determined by a stress intensity factor range. From a material science perspective, fatigue crack propagation behaviour of materials has been considered through "intrinsic" and "extrinsic" mechanisms,[3] where "intrinsic" mechanisms concern with the formation of new fracture surfaces; whilst "extrinsic" mechanisms consider "shielding" effects due to various mechanisms of crack closure. From an engineering perspective, fatigue crack growth may be considered as "primary events" occur ahead of the crack tip and "secondary events" occur behind the crack tip. At a local level, for crack growth to occur, the material ahead of a crack tip must separate, hence a local mechanical driving force ought to be of

much interest. However, although mechanisms for material separation in various material systems have been studied in some detail, progress towards a quantitative measure of micro-crack driving force for fatigue crack growth[2] is still lacking.

Fatigue crack closure is a well-known phenomenon first reported by Elber[4] in a study of crack growth under cyclic tension loading. He observed that a crack may be partially closed when subjected to cyclic tensile loads.[4] His work prompted extensive research on fatigue crack closure, with the main types of crack closure discussed in a recent comprehensive review.[5] A general feature of crack closure[6] is a change of stiffness in the load against displacement curves, marked by a "knee" in the measured compliance during loading and unloading, which is considered to be indicative of "crack opening", from which K_{op} may be estimated and an "effective" stress intensity factor ΔK_{eff} ($K_{max} - K_{op}$) may be obtained. Since K_{op} is usually larger than K_{min} for tension-tension cycles at low load ratios, ΔK_{eff} is usually smaller than the applied ΔK. Numerous empirical formulations have been proposed to quantify $K_{op,}$ notably as a function of load ratio. [6] Considerable work has since been carried out to utilise the concept of crack closure to explain or rationalise a wide range of fatigue crack growth data, with an estimated some 10,000 papers published since Elber.[5] In particular, plasticity-induced crack closure has been used as the default interpretation of load ratio effects, and the concept has been incorporated in some fatigue life prediction models. However, despite some doubts expressed over the role of crack closure in affecting fatigue crack growth rates,[7-9] there are no systematic studies with experimental evidence to support that the change in the compliance recorded behind the crack tip during loading/unloading has definitive "attenuation" effects on the stresses/strains in the near-field ahead of the crack tip, or the stress intensity factor range ΔK globally. There is a need to revisit the phenomenon of crack closure and its impact on fatigue crack growth, so that damage tolerance life management can be more robust and physical-based, hence applicable to more complex service loading conditions.

In this work, we have utilised Digital Image Correlation (DIC) to examine, *in situ*, the full-field displacements and strains around a fatigue crack tip. A model material, stainless steel 316L, was used in compact tension (CT) specimens and tested under cyclic loading with a load ratio of 0.1. Normal strains ahead of the crack tip, considered particularly relevant to crack growth,[10-14] were measured during loading/unloading; whilst crack opening displacements (COD) were measured behind the crack tip at selected distances to the crack tip. Two spatial resolutions were adopted to obtain both micro and macro responses. The stress intensity factor K was estimated from the displacement data obtained from DIC,[15] and compared with the nominal values during loading.

We hope that the results will provide a first concurrent experimental evidence of crack closure behind the crack tip, near-tip strains ahead of the crack tip and the stress intensity factor determined by the measured displacement field. The information will provide insights into the nature of crack closure and its relevance to fatigue crack growth.

METHODS

Material & Specimen

The material studied is stainless steel 316L, which has a yield stress of 280 MPa, an elastic modulus of 193 GPa and a Poisson's ratio of 0.3. A standard compact tension (CT) specimen (ASTM E647, Width W=60 mm, thickness B=7 mm) was used, with a machined notch size of 12 mm. Prior to mechanical testing, the surface of the specimen was etched to expose the microstructure features, and an average grain size was measured as approximately 17 μm.

Mechanical testing

Mechanical testing was carried out on an Instron servo-hydraulic testing machine (25kN). Pre-cracking was carried out under load-control using a load shedding scheme. The initial ΔK was 25 MPa$\sqrt{m}$, and the load was reduced manually step-by-step based on the measured crack length. The load ratio and loading frequency were 0.1 and 10 Hz, respectively. Crack growth was monitored by both direct current potential-drop (DCPD) technique and surface replicas. The latter readings were taken as the true surface crack lengths; whilst the crack lengths from DCPD readings are indicative of the average crack lengths from which the nominal mode I stress intensity factor values were calculated for testing purposes. The pre-cracking was terminated when the crack length reached a/W ≈ 0.4, $\Delta K \approx 15$ MPa$\sqrt{m}$. Mechanical testing was then carried out under cyclic load (R=0.1) at ΔK = 15, 20, 25 MPa$\sqrt{m}$. About 100 cycles were allowed to elapse before imaging after the load was raised to the next level, and three cycles were recorded at each load level. The loading waveform was trapezoidal, with a 20 second loading/unloading and a 4 second hold at minimum and maximum loads during image acquisition. Within each load cycle, 48 images were collected during loading/unloading at a frequency of one image per second. Optical microscopy was used also to monitor the crack length, and to verify the crack tip position. Negligible crack growth was found at ΔK=15, 20 MPa$\sqrt{m}$; whilst about 10 μm crack growth was detected at ΔK=25 MPa$\sqrt{m}$, which was considered sufficiently small not to invalid the assumption of stationary cracks.

DIC image capture

For the micro-DIC analysis, a random speckle pattern was applied directly onto one of the specimen surfaces using graphite powder. The random speckle pattern generated may be described by its grey level intensity profile, which has a bell-shaped distribution and is deemed appropriate for image correlation purposes. The imaging system (LAVISION, GMBH) consisted of a CCD camera (2456 × 2058 pixels) and a Schneider Kreuznach F2.8 50mm lens with 100mm extension tubes. A field of view (FOV), a rectangle of 1.2mm×1.1mm (FOV_1) with the crack tip in the centre, was selected for imaging in order to capture the near-tip strain data ahead and COD data behind the crack tip. A spatial resolution of 0.5 μm/pixel was achieved. For the macro-DIC analysis, a CCD camera (2456 × 2058 pixels) was used and images were taken of the speckle patterns generated on a painted white specimen surface. A FOV of 7.5mm×6mm (FOV_2) was used, resulting a spatial resolution of 3.1μm/pixel. The latter was necessary to obtain the data away from the plastic zone (estimated up to 1.3mm), permitting regression analysis to obtain K at higher loads from the displacement

data. To carry out DIC imaging using FOV_2, the specimen was loaded cyclically using a load shedding scheme, as in pre-cracking, till sufficient crack growth obtained at each step and ΔK=15 MPa$\sqrt{m}$ and a/W≈0.4 were achieved at the final step, when DIC imaging was repeated as before at ΔK=15, 20, 25 MPa$\sqrt{m}$. DaVis StrainMaster (Version 8.4) was used for image correlation and the calculation of strains.

DIC measurement uncertainties were assessed using the images collected under zero load to estimate the baseline errors for both displacements and strains. The influence of processing parameters on the measurement errors was also evaluated. The displacements were obtained at the selected stages of a cycle by correlating the deformed images at a given load level and a reference image taken at minimum loads. No filter was used in the data processing. The strain values were obtained, without smoothing, by direct approximation of displacement gradients between the neighbouring vectors in x and y directions. A subset size of 59 pixels by 59 pixels, with a step size of 14 pixels; and a strain measurement window of 15 µm by 15 µm were used to calculate the displacements and strains for both micro-DIC and macro-DIC analysis. The standard deviations for normal displacements are 0.012 µm (FOV_1) and 0.025 µm (FOV_2); and 0.068% (FOV_1) and 0.022% (FOV_2) for normal strains, respectively. For conciseness only normal components are reported here.

The setup for mechanical testing and DIC image capture is shown in Figure 1.

Determination of SIF from DIC data

The mode I stress intensity factor K_I was obtained by fitting the displacement data obtained from the DIC to the Williams' series expansion[15] using an algorithm DICITAC[16]. According to Williams[15], the displacement field ahead of a crack tip may be expressed as infinite series, which may be written as follows:[16]

$$u(r,\theta) = \sum_{n=0}^{N} \frac{1}{2\mu} a_n r^{\frac{n}{2}} \times \left\{ \left(\kappa + \frac{n}{2} + (-1)^n \right) \cos\frac{n\theta}{2} - \frac{n}{2} cos\left(\frac{n}{2} - 2\right)\theta \right\} + \sum_{n=0}^{M} \frac{1}{2\mu} b_n r^{\frac{n}{2}} \times \left\{ \left(-\kappa - \frac{n}{2} + (-1)^n \right) \sin\frac{n\theta}{2} + \frac{n}{2} sin\left(\frac{n}{2} - 2\right)\theta \right\} \quad (1)$$

$$v(r,\theta) = \sum_{n=0}^{N} \frac{1}{2\mu} a_n r^{\frac{n}{2}} \times \left\{ \left(\kappa - \frac{n}{2} - (-1)^n \right) \sin\frac{n\theta}{2} + \frac{n}{2} sin\left(\frac{n}{2} - 2\right)\theta \right\} + \sum_{n=0}^{M} \frac{1}{2\mu} b_n r^{\frac{n}{2}} \times \left\{ \left(\kappa - \frac{n}{2} + (-1)^n \right) \cos\frac{n\theta}{2} + \frac{n}{2} cos\left(\frac{n}{2} - 2\right)\theta \right\} \quad (2)$$

where u and v are displacements in x and y directions; a_n and b_n are related to mode I and mode II parts of deformation, respectively. μ is the shear modulus and κ = (3-ν)/(1+ν) for plane stress, ν is the Poisson's ratio; r is the radial distance from crack tip and θ is the phase angle in a polar coordinate system with the crack tip at the centre. The displacement data from the DIC measurements were first processed to remove rigid body motions using

LaVision StrainMaster (v 8.4), then fitted to six terms of Williams' series[15] to obtain the values of K_I as a function of applied load, further details of the fitting procedure were given elsewhere.[16] The fitting strategies, including the appropriate area of interest, the subset size and the size of the measurement window recommended in[17] were considered and adopted as appropriate. Specifically, a rectangular region of 1.28 x 1.07 mm^2 (FOV_1) and 7.5 x 5.9 mm^2 (FOV_2) were chosen as areas of interest (AOI) to perform image correlation. The crack length was about 1/3 inside of the AOI (between 25% to 50% recommended). A subset size of 49 pixels × 49 pixel, and a step size of 6 pixels were used. The AOIs contain approximately 115,000 displacement data points.

RESULTS

The full-field information around the crack tip is presented based on a schematic shown in Figure 2. Tracking points were used for recording the CODs in the crack wake and normal strains ahead of the crack tip, with 0 indicating the position of the crack tip. The tracking points were chosen to be multiples of the average grain size (Δ=17 μm). An area over the crack wake was masked to avoid the discontinuity giving rise to non-correlation in the DIC analysis. The CODs were calculated based on the relative vertical displacements of A_{1i} and A_{2i} for the selected points at the selected distances to the crack tip (i = 1Δ, 2Δ, 4Δ and 10Δ); whilst the vertical distance between A_{1i} and A_{2i} was taken as 30 μm, as trials show that varying this distance has negligible effects on the measured CODs. An area of 15μm×15μm was used as the measurement window to calculate the strains at the selected tracking points j (=1Δ, 2Δ, 3Δ, 4Δ). Only normal strains are presented for clarity, as they are most relevant to crack growth. [11,12] Figure 3 shows a typical displacement and strain map taken under K = 22 MPa√m.

Normal strains ahead of the crack tip

The measured normal strains ahead of the crack tip from the micro-DIC (FOV_1) are shown in Figure 4 (a-c) during loading (similar results obtained for unloading, omitted) under ΔK=15, 20, 25 MPa√m, at the selected distances to the crack tip (1Δ, 2Δ, 4Δ and 10Δ, Δ=17 μm). Significant scatters are obtained away from the crack tip and at low ΔK, although a trend of increasing normal strain with the increase of load is evident, particularly close to the crack tip (1-2 grain sizes). Figure 5 shows the normal strains as a function of applied load under the three load cases at the selected positions to the crack tip, showing more clearly the effects of loading on the near-tip normal strains, particularly at distances close to the crack tip. There appears to be no discontinuity or a "knee" during loading or unloading, except at the first couple of positions near the crack tip under ΔK=15 MPa√m, where the strain appears to be consistently low till P/P_{max}>0.6. Further work from macro-DIC (FOV_2) shows, however, a trend of continuous increase in normal strain with the increase of load at ΔK=15 MPa√m also (Figure 4(d)), suggesting that efficient load transfer to the near-tip strain field occurred during loading, and no stress "shielding" effects during loading or unloading are found ahead of the crack tip.

Crack Opening Displacement

Both micro and macro DICs were carried out to measure the crack opening displacement (COD) using FOV_1 and FOV_2 at the selected distances to the crack tip (1-10Δ, 500 μm) and at the three ΔK levels. The CODs were calculated from the vertical displacements of A_{1i} and A_{2i} at a fixed distance to the crack plane y=30 μm (Figure 2). The micro-DIC results are presented in Figure 6(a)-(c) and Figure 7; whist macro-DIC results at ΔK=15 MPa√m are presented in Fig 6(d). Significant crack closure, as identified by the change of slope in the P/P_{max} vs COD curves, is evident at ΔK=15 MPa√m), although the "opening" level appears to vary with the measurement resolution (Fig 6(a), (d)). Also, the level of closure is reduced progressively as ΔK is increased (Fig 6(a)-(c)). Figure 7 shows the loading and unloading loops at the selected distances to the crack tip for the three load cases. A "knee" can be observed in most cases, although not at a constant value of P_{op}/P_{max}. Considerably more crack closure can be observed at ΔK=15 MPa√m ($P_{op}/P_{max} \approx 0.6$) than that at ΔK=20 MPa√m ($P_{op}/P_{max} \approx 0.4$) and 25 MPa√m ($P_{op}/P_{max} \approx 0.2$). Figure 8 shows a summary of P_{op}/P_{max} as a function of the distance to the crack tip from both micro and macro DIC analyses using FOV_1 and FOV_2. The variations of P_{op} with the distance to the crack tip and load level are evident. Generally, higher P_{op} is observed closer to the crack tip than that away from the crack tip, and relatively constant values of P_{op} are obtained away from the crack tip, although these stabilised values depend strongly on the applied ΔK. Interestingly, the influence of the size of FOV on the measured opening load seems to be significant. At ΔK=15 MPa√m, $P_{op}/P_{max} \approx$ 0.46-0.55 is obtained at low resolution (FOV_2), as opposed to $P_{op}/P_{max} \approx$ 0.61-0.67 at high resolution (FOV_1); at ΔK=20 MPa√m, $P_{op}/P_{max} \approx$ 0.16-0.18 is obtained at low resolution (FOV_2), as opposed to $P_{op}/P_{max} \approx$ 0.36-0.44 at high resolution (FOV_1); and at ΔK=25 MPa√m, $P_{op}/P_{max} \approx$ 0.15-0.18 is obtained at low resolution (FOV_2), as opposed to $P_{op}/P_{max} \approx$ 0.18-0.28 at high resolution (FOV_1). These variations in the measured P_{op} present significant difficulties in the use of an "effective" ΔK, even at a low K level where crack closure clearly presents. At higher K (ΔK≥20 MPa√m), there seems very little evidence of "crack closure" in the stiffness change. This casts some doubts on the perceived role of crack closure during steady-state fatigue crack growth, characterized normally by Paris Law.

Stress Intensity Factor estimated from DIC data

Stress Intensity Factor K was obtained by fitting the measured DIC displacement data to the Williams' series expansion[15], using an algorithm[16] developed at Sheffield. The larger FOV_2 (7.5mm×6mm) was used to fit all three cases. This was necessary to accommodate the plasticity near the crack tip at ΔK≥20 MPa√m, where the total strain measured by DIC contains a significant plastic component which would otherwise produce artificially high K values using FOV_1. According to Irwin's estimate, the maximum monotonic plastic zone ahead of the crack tip under plane stress conditions is about 1.3 mm at ΔK=25 MPa√m, sufficient data away from the near-tip plasticity are available in FOV_2 for accurate fitting of K for all three cases.

Figure 9 shows the values of fitted K_I for the three load cases using FOV_2, together with the nominal K_I values for the CT specimen. "Crack opening" estimated from the K vs P/P_{max} curves appears to be around 0.2, a value broadly consistent with the opening load P_{op}

identified from the COD vs P/P_{max} curves at this resolution (Figure 8: ΔK=20 MPa$\sqrt{m}$, P_{op}/P_{max} ≈ 0.16-0.18; ΔK=25 MPa$\sqrt{m}$, P_{op}/P_{max} ≈ 0.15-0.18); but lower than that for ΔK=15 MPa$\sqrt{m}$ (P_{op}/P_{max} ≈ 0.46-0.55). The opening level from the estimated K values is much lower than all those estimated from COD vs P/P_{max} curves using FOV_1. For ΔK=15 MPa$\sqrt{m}$, K was also estimated using the displacement data obtained at high resolution (FOV_1), and crack opening was found to be around 0.6, a value comparable with the P_{op}/P_{max} measured from the COD vs P/P_{max} curve (Figure 6a).

DISCUSSION

The use of DIC to evaluate microscale displacements and strains near a fatigue crack tip was first reported by Sutton et al[18] in 1999. Crack opening was measured at two locations (75 µm and 224 µm) behind the crack tip for AA8009 steel alloy at ΔK=4.4 MPa$\sqrt{m}$ (R=0.05). Higher value of P_{op}/P_{max} (≈ 0.26) was obtained at 75 µm than that at 224 µm to the crack tip (P_{op}/P_{max} ≈ 0.15). Carroll et al[19] used the DIC method to examine crack opening in both macro and micro scales at three stress intensity factor ranges (9.7, 15.4 and 18.9 MPa$\sqrt{m}$) in a Grade 2 Titanium. Their results show that crack opening P_{op}/P_{max} varies with the location of the measurement gauge, load level and the measurement resolution. Crack opening load increases with the reduction of the distance to the crack tip; decreases with the reduction of the measurement magnification, with P_{op} found between 5-15% at 3.9 µm/pixel and 15-30% at 0.33 µm/pixel of P_{max}. There appeared to be little crack closure at ΔK=18.9 MPa$\sqrt{m}$, although they used three different specimens and argued that the short crack with regard to the notch length in this specimen was attributed to the latter observation. O'Connor et al[20] conducted both macro and micro DIC analysis of the near-tip displacements and strains using a 6082-T6 aluminium alloy. They also showed that the opening load is higher for locations closer to the crack tip, as the crack peels open from the mouth towards the tip. For constant amplitude fatigue, the fitted K using the displacement data from DIC broadly followed the analytical K, although with an offset, which they attributed to crack closure due to an additional negative residual K.

In the present work, we have carried out macro and micro DIC analysis to obtain *full-field* information around a fatigue crack tip, both ahead and behind the crack tip, using the *same* specimen under three load cases. The surface measurements captured a worst-case scenario, where a plane stress condition is known to favour plasticity-induced crack closure, and its impact on the full-field near-tip strains can therefore be assessed simultaneously and systematically. The evolution of the normal total strain ahead of the crack tip is reflective of the primary events; whilst CODs are indicative of secondary events. The fitted K using the full-field displacements may be considered as a global "effective" crack driving force, reflective of the overall stress state around the crack tip.

The influence of DIC parameters on the fitted K from the measured displacements was examined in Mokhtarishirazabad et al[17]. Significant effects of field of view, area of interest and subset size on the fitted K were illustrated and recommendations were made with regard to the selection of these parameters. The influence of DIC processing parameters on the results was considered in this work, where the subset size, step size and measurement window were kept constant throughout both micro and macro DIC analyses. A larger field

of view was used to accommodate the extensive plasticity near the crack tip, although the plastic zone region was not excluded in the fitting of K.[17]

Currently, there is *no consensus* on the role of "crack closure" in regulating the process of fatigue crack growth. Although the phenomenon of plasticity-induced crack closure is well reported, the true effects of such on the crack driving force or the crack tip stress/strain fields are largely unknown. Systematic studies have not been possible till recently, when full-field techniques such as DIC become more widely available. We have utilised DIC to interrogate this experimentally, and both primary and secondary events ahead and behind of the crack tip were measured simultaneously. Specifically, new information has come to light from this study: i) Crack opening (P_{op}/P_{max}) *decreases* with the decrease in measurement resolution, the increase in the distance to the crack tip and the increase in load level, hence "crack opening" cannot be considered a unique or a constant value; ii) there appears to be little evidence of crack closure from the measured K vs load; and the values of P_{op} do not correlate with the measured changes in K during loading; iii) the near-tip normal strains are found to increase continuously with the increase of the applied load, and do not correlate with the trend presented in the COD vs load curves. The lack of uniqueness of "crack opening" is consistent with the results of Carroll et al[19] and others.[18, 20] Unlike in Carroll et al,[19] however, the same specimen was used throughout our experiments, hence no ambiguities in the results presented.

CONCLUDING REMARKS

In this work, we have utilised DIC to measure, *in situ,* the surface crack opening displacement (COD) at selected locations behind the crack tip and the evolution of the near-tip displacements and strains ahead of the crack tip during loading and unloading in a model material. The stress intensity factor for the CT specimen was estimated from the Williams' series expansion using the displacements recorded by DIC as a function of the applied load. The results present a more complete picture of the crack tip field, where events both ahead and behind of the crack tip were examined and discussed in terms of crack driving and attenuation effects.

A classic case of crack problem under plane stress loading condition was examined, where crack closure is known to be significant. Our results show that even where closure is identified, its impact on the global crack driving force K seems to be small. Furthermore, there appears to be no impact of crack closure on the near-tip normal strains ahead of the crack tip. Admittedly, our study was based on one material at selected loading conditions. Further work is needed to study the phenomenon in other materials and loading systems. Nevertheless we hope that the results provide some fundamental insights into the full-field behaviour of a crack tip under cyclic loading conditions; and shed light on the phenomenon of crack closure and its relevance to crack driving force ΔK for steady-state fatigue crack growth. Caution should be taken against routine treatments of an "effective" ΔK by considering crack closure in the characterization of fatigue crack growth, till such a time when more evidence emerges to either support, or against, this line of argument.

ACKNOWLEDGEMENTS

SA is supported by a scholarship from Saudi Arabia Government. DICITAC was developed by Dr M. Zanganeh during his PhD studies at the University of Sheffield.

REFERENCES

1. Paris PC, Gomez MP, Anderson WE. A rational analytic theory of fatigue. *Trend Eng.* 1961;13:9–14.
2. Rice JR. Mechanics of Crack Tip Deformation and Extension by Fatigue. *Fatigue Crack Propagation.* 1967;ASTM STP 4:247–309.
3. Ritchie RO. Mechanisms of fatigue crack propagation in metals, ceramics and composites: Role of crack tip shielding. *Mater Sci Eng.* 1988;103:15–28.
4. Elber W. Fatigue Crack Closure Under Cyclic Tension. *Eng Fract Mech.* 1970;2:37–45.
5. Pippan R, Hohenwarter A. Fatigue crack closure: a review of the physical phenomena. *Fatigue Fract Eng Mater Struct.* 2017;40:471–95.
6. Suresh S. Fatigue of Materials: 2nd ed. Cambridge: Cambridge University Press; 1998.
7. McEvily AJ. On Crack Closure in Fatigue Crack Growth. Mech Fatigue Crack Closure, ASTM STP 982, 1988:35–43.
8. Louat N, Sadananda K, Duesbery M, Vasudevan AK. A Theoretical Evaluation of Crack Closure. *Metall Trans A.* 1993;24:2225–32.
9. Vasudeven AK, Sadananda K, Louat N. A review of crack closure, fatigue crack threshold and related phenomena. *Mater Sci Eng A.* 1994;188:1–22.
10. Zhao LG, Tong J, Byrne J. The evolution of the stress – strain fields near a fatigue crack tip and plasticity-induced crack closure revisited. *Fatigue Fract Engng Mater Struct.* 2004;27:19–29.
11. Zhao LG, Tong J. A viscoplastic study of crack-tip deformation and crack growth in a nickel-based superalloy at elevated temperature. *J Mech. Physics Solids*. 2008; 56:3363-3378.
12. Tong J, Lin B, Lu YW, Madi K, Tai YH, Yates JR, et al. Near-tip strain evolution under cyclic loading: In situ experimental observation and numerical modelling. *Int J Fatigue.* 2015;71:45–52.
13. Lu Y-W, Lupton C, Zhu M-L, Tong J. In Situ Experimental Study of Near-Tip Strain Evolution of Fatigue Cracks. *Exp Mech.* 2015;55:1175–85.
14. Zhu ML, Lu YW, Lupton C, Tong J. In situ near-tip normal strain evolution of a growing fatigue crack. *Fatigue Fract Eng Mater Struct.* 2016;39:950-955.
15. Williams ML. On the Stress Distribution at the Base of a Stationary Crack. *J Appl Mech.* 1957;24:109–14.
16. Yates JR, Zanganeh M, Tai YH. Quantifying crack tip displacement fields with DIC. *Eng Fract Mech.* 2010;77:2063–76.
17. Mokhtarishirazabad M, Lopez-Crespo P, Moreno B, Lopez-Moreno A, Zanganeh M. Evaluation of crack-tip fields from DIC data: A parametric study. *Int J Fatigue.* 2016;89:11–9.
18. Sutton MA, Orteu JJ, Schreier H. Image correlation for shape, motion and deformation measurements: Basic concepts, theory and applications. Springer US, 2009.

19. Carroll J, Efstathiou C, Lambros J, Sehitoglu H, Hauber B, Spottswood S, et al. Investigation of fatigue crack closure using multiscale image correlation experiments. *Eng Fract Mech.* 2009;76:2384–98.
20. O'Connor SJ, Nowell D, Dragnevski KI. Measurement of fatigue crack deformation on the macro- and micro-scale: Uniform and non-uniform loading. *Int J Fatigue.* 2016;89:66–76.

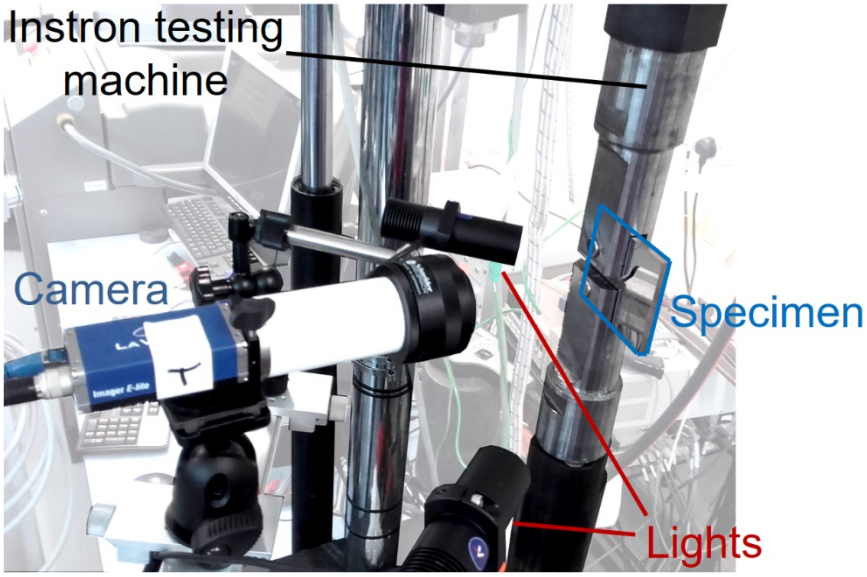

Figure 1. The experimental setup for cyclic testing and DIC imaging.

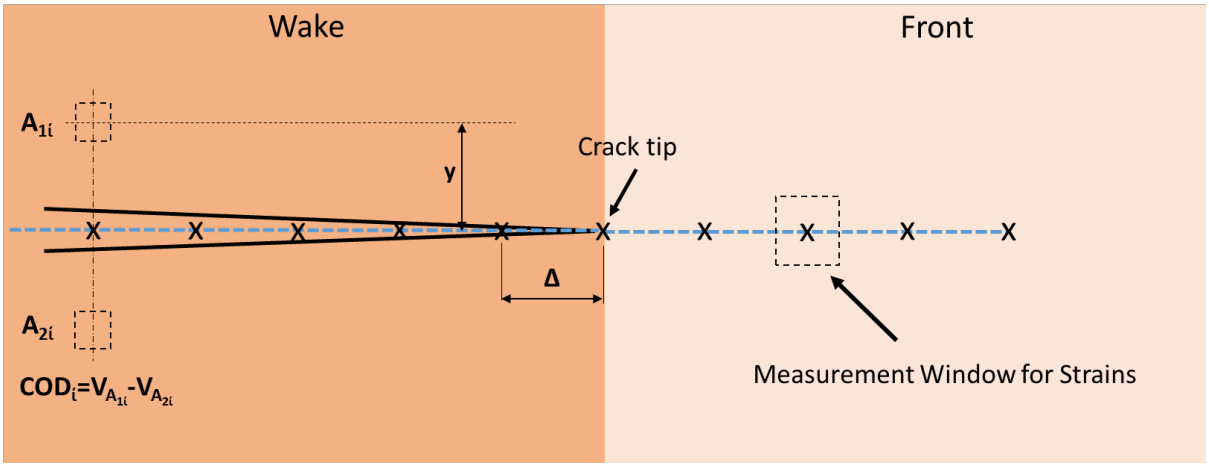

Figure 2. An illustration of the tracking points used for recording the normal strains ahead of the crack tip (Front: íΔ, í=1, 2, 4, 10) and the CODs in the crack wake (Wake: íΔ, í=1, 2, 4, 10, 29). The tracking points were chosen to be multiples of the average grain size (Δ = 17 µm). The CODs were calculated from the vertical displacements of $A_{1í}$ and $A_{2í}$ at a fixed distance to the crack plane y (30 µm); the measurement window for strain calculation is 15 µm by 15 µm.

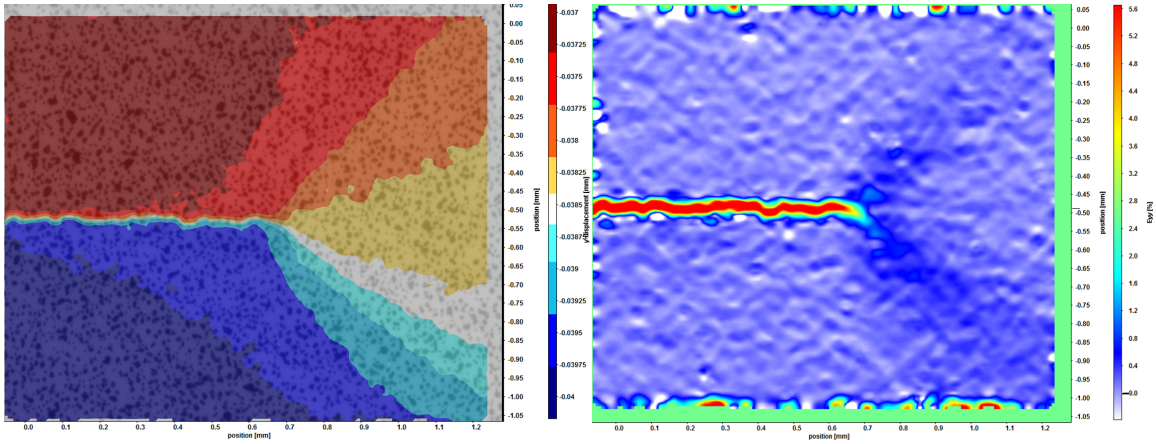

(a) (b)

Figure 3. A typical map of (a) displacement V_{yy} and (b) strain ε_{yy} (taken at K = 22 MPa√m).

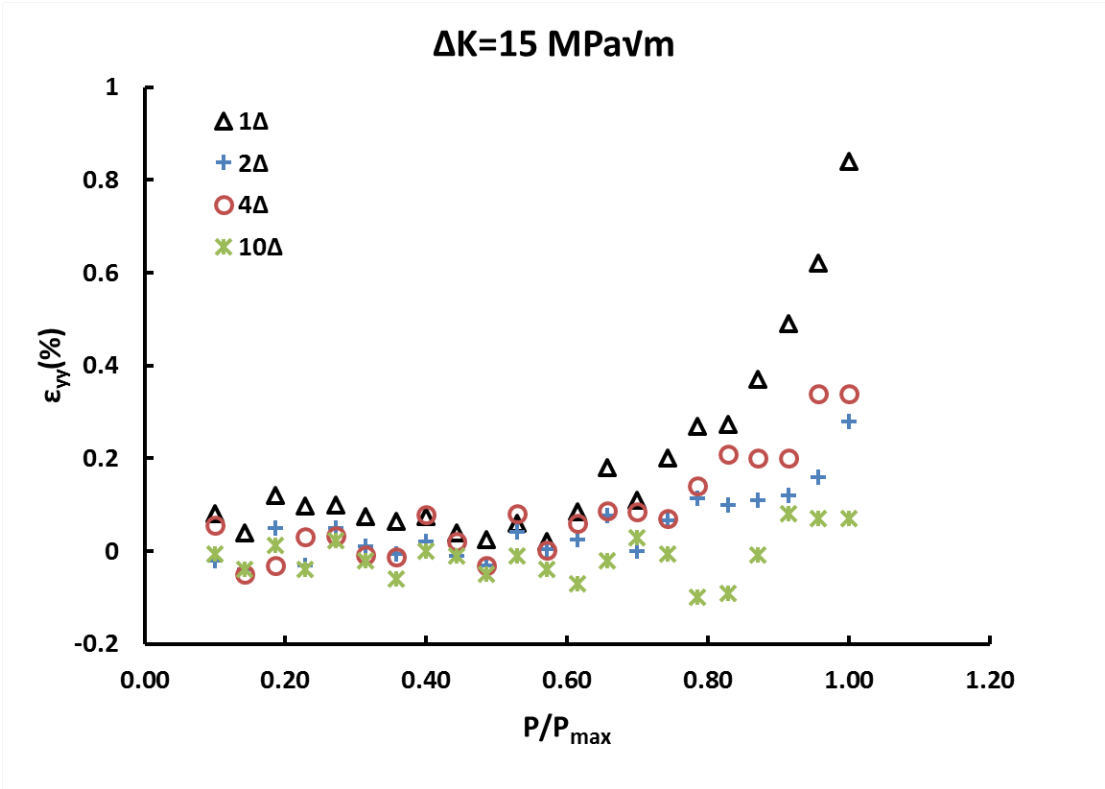

(a)

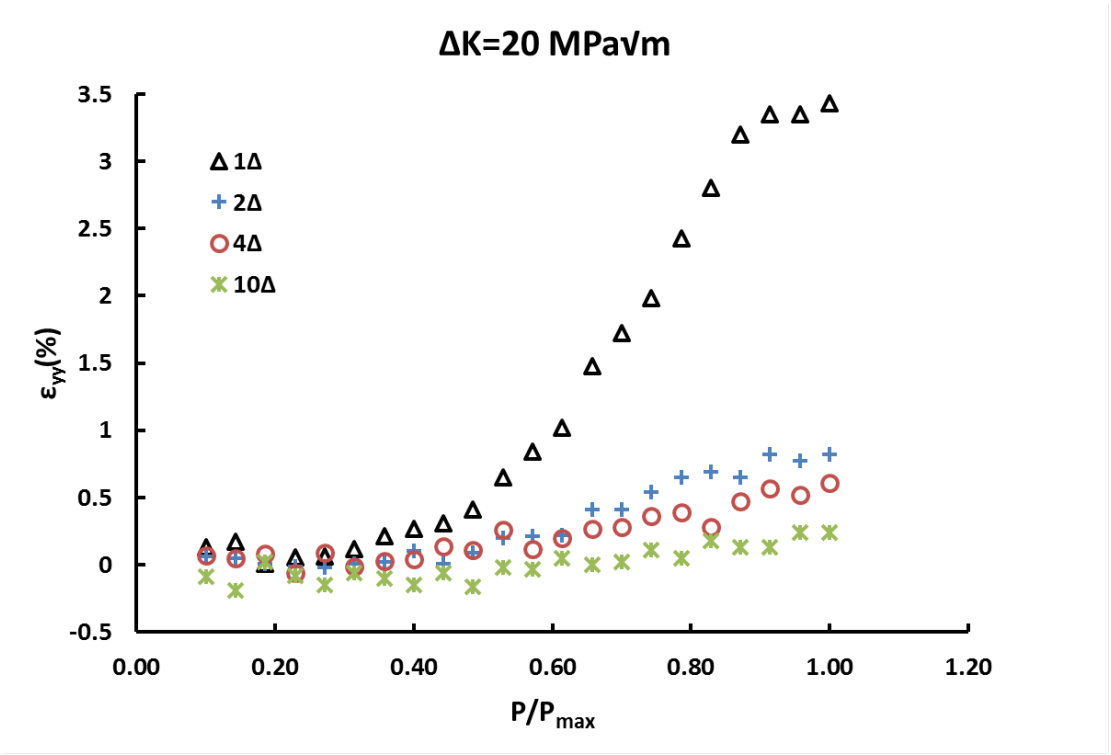
ΔK=20 MPa√m
1Δ
2Δ
4Δ
10Δ
ε_{yy}(%)
P/P$_{max}$
3.5
3
2.5
2
1.5
1
0.5
0
-0.5
0.00
0.20
0.40
0.60
0.80
1.00
1.20

(b)

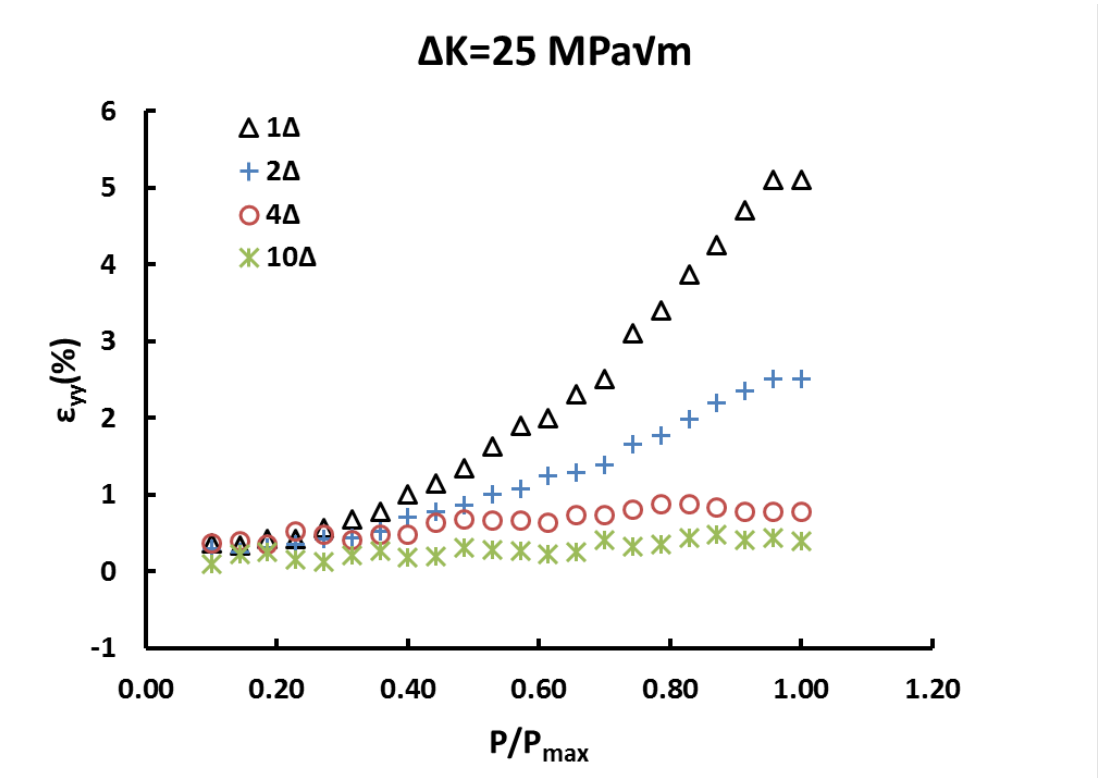
ΔK=25 MPa√m
1Δ
2Δ
4Δ
10Δ
ε_{yy}(%)
P/P$_{max}$
6
5
4
3
2
1
0
-1
0.00
0.20
0.40
0.60
0.80
1.00
1.20

(c)

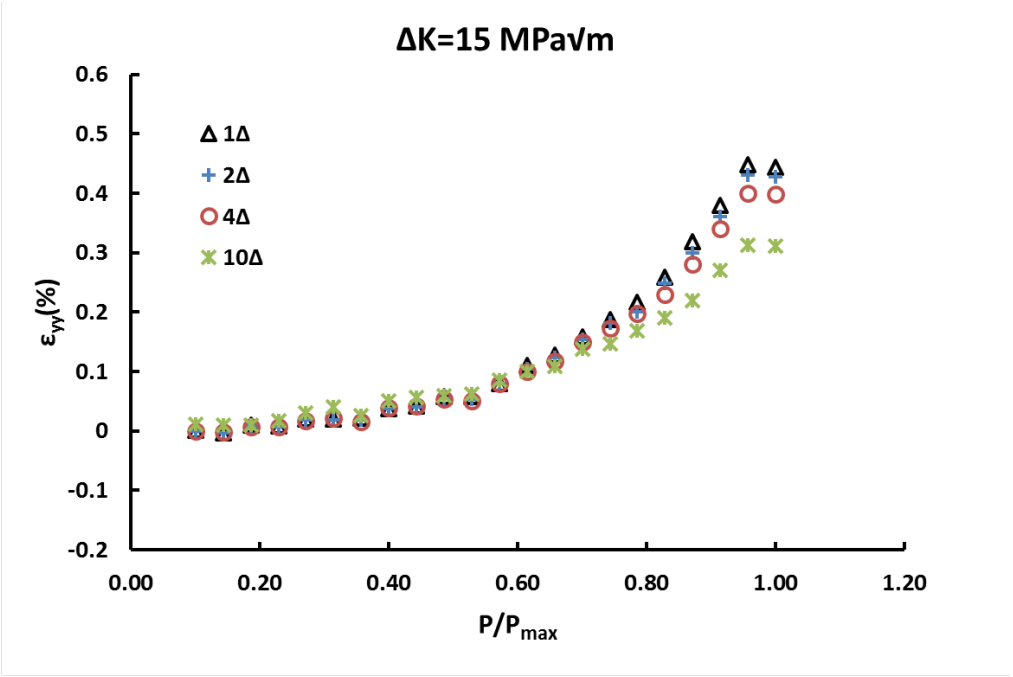

(d)

Figure 4. The normal strains measured at the selected locations ahead of the crack tip for the three load cases (a-c) using FOV_1 and (d) at ΔK=15 MPa√m using FOV_2.

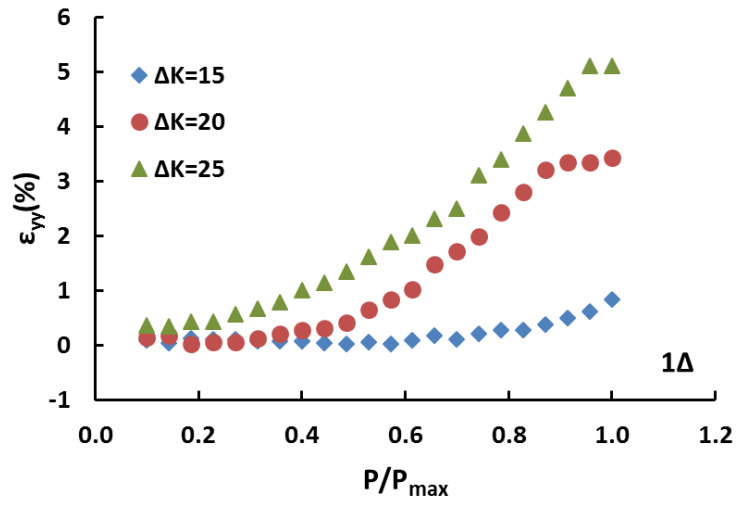

(a)

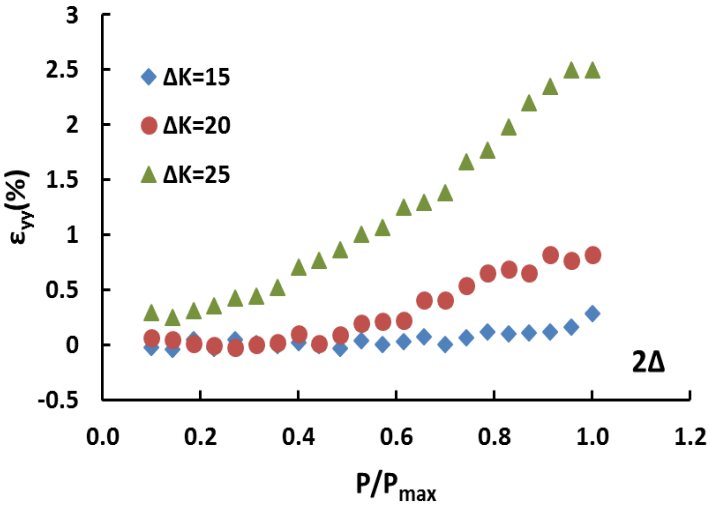

(b)

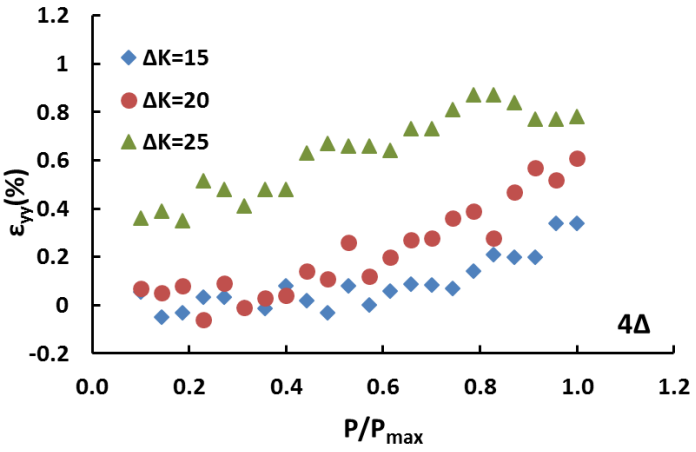

(c)

Figure 5. The effects of load level on the strain development at the selected locations (a: Δ; b: 2Δ; c: 4Δ) ahead of the crack tip (FOV_1).

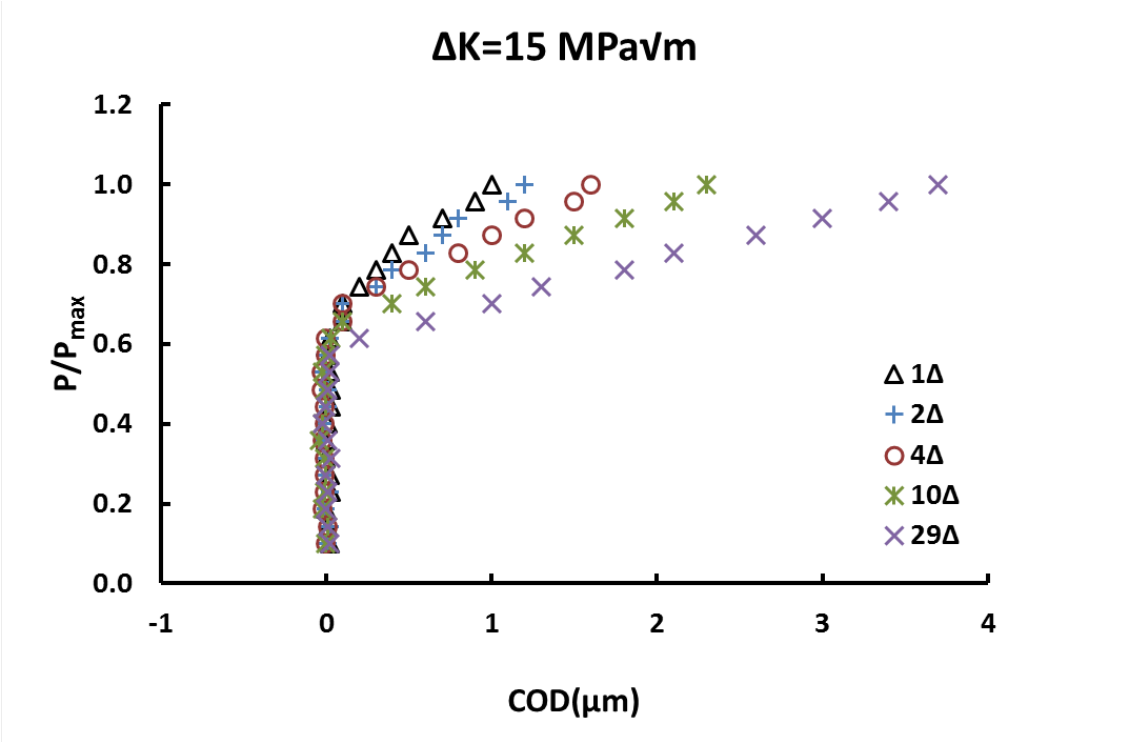

(a)

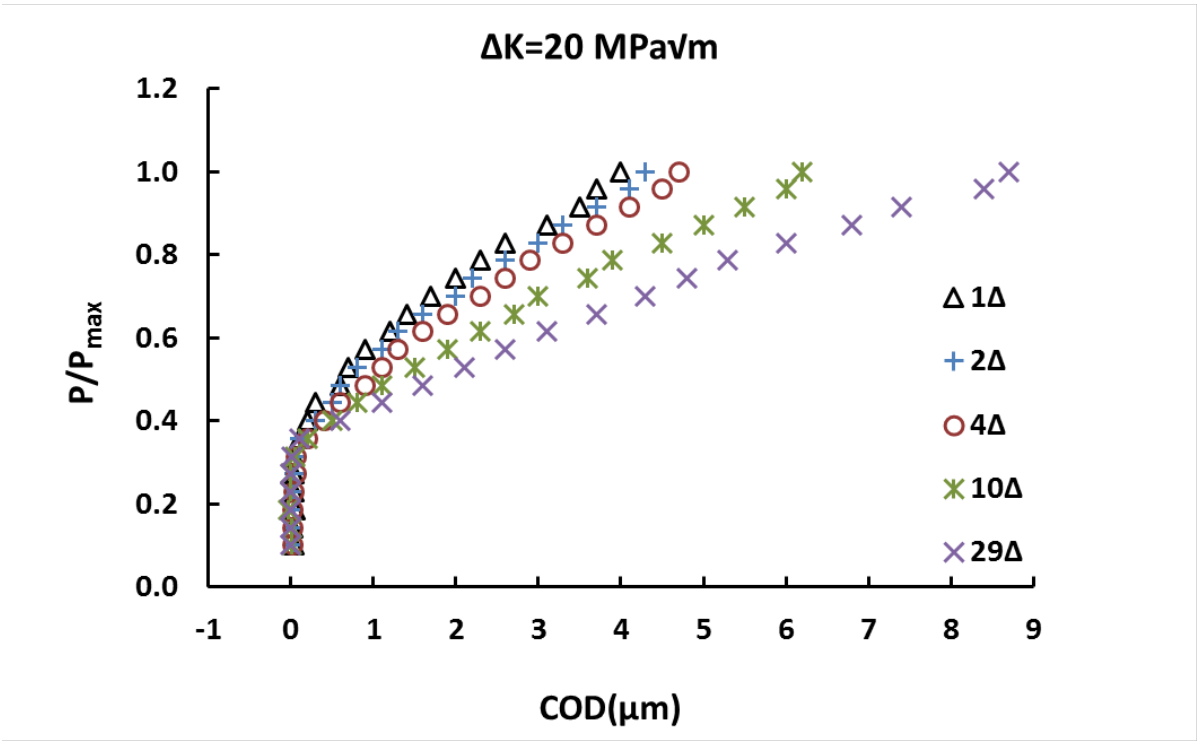
ΔK=20 MPa√m
P/P max
COD(μm)
1Δ
2Δ
4Δ
10Δ
29Δ

(b)

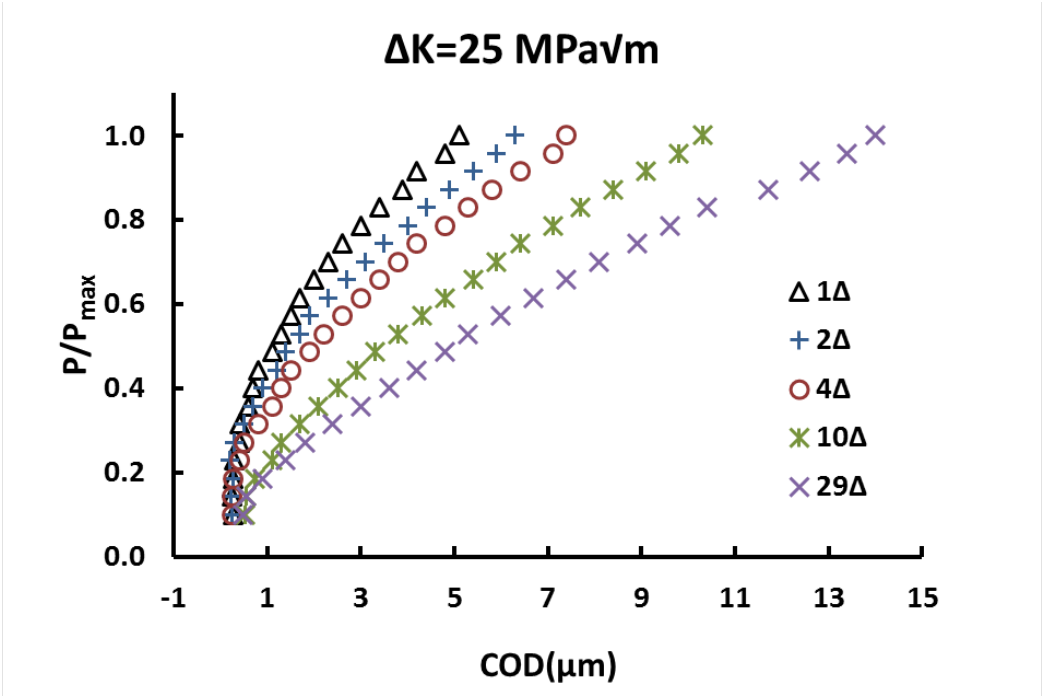
ΔK=25 MPa√m
P/P max
COD(μm)
1Δ
2Δ
4Δ
10Δ
29Δ

(c)

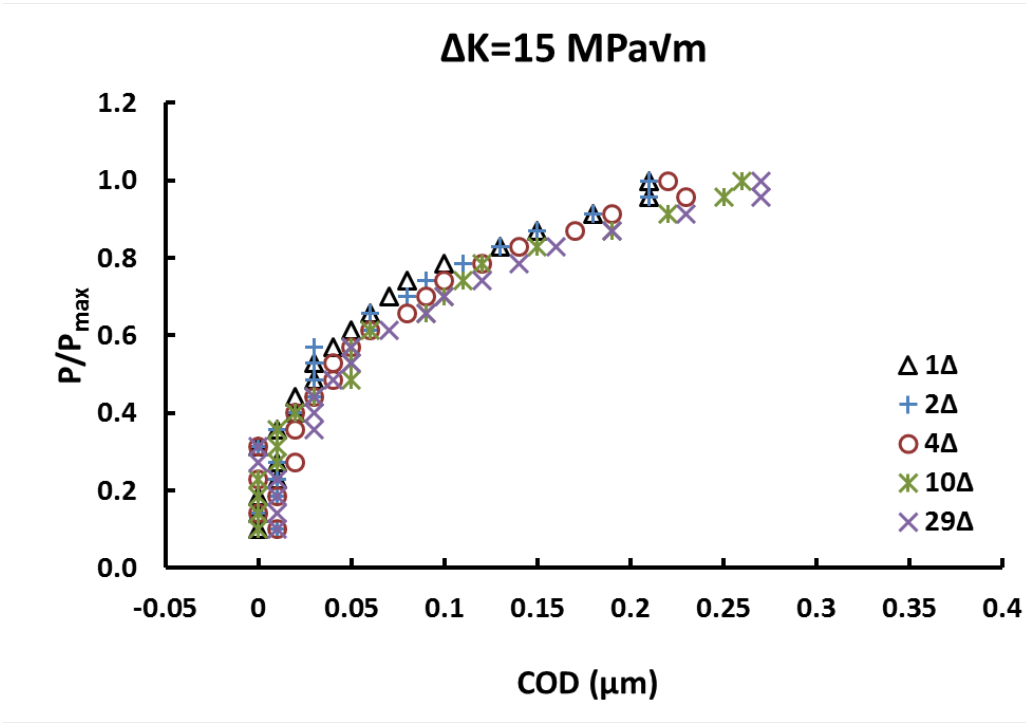

(d)

Figure 6. The CODs measured at the selected locations along the crack flanks for the three load cases (a-c, FOV_1) and (d) at ΔK=15 MPa√m using FOV_2.

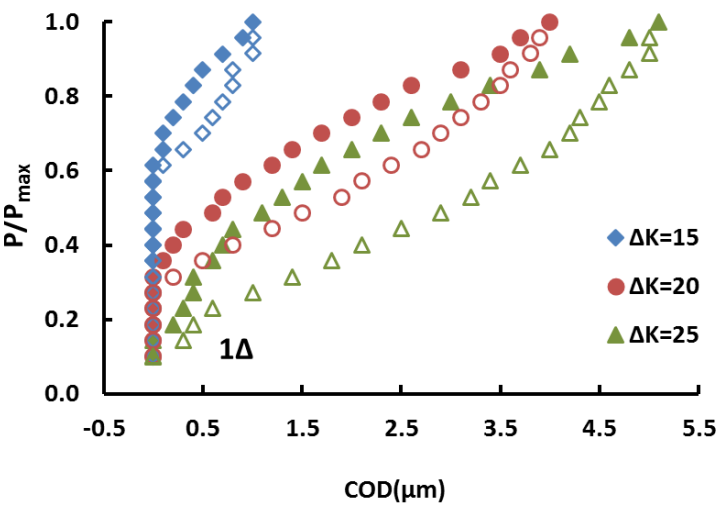

(a)

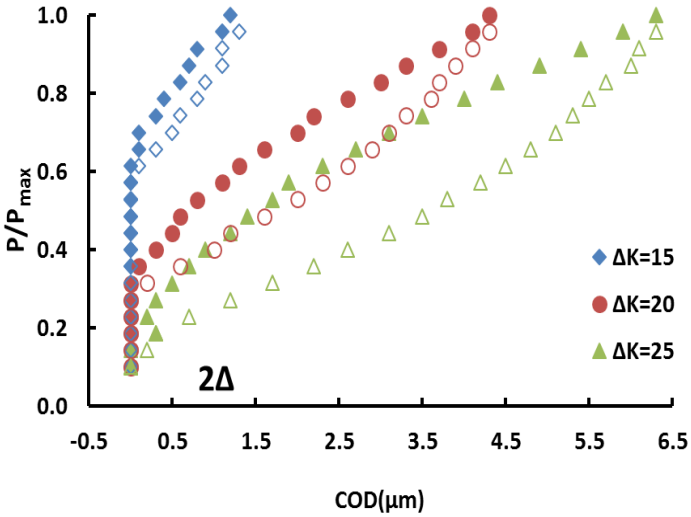

(b)

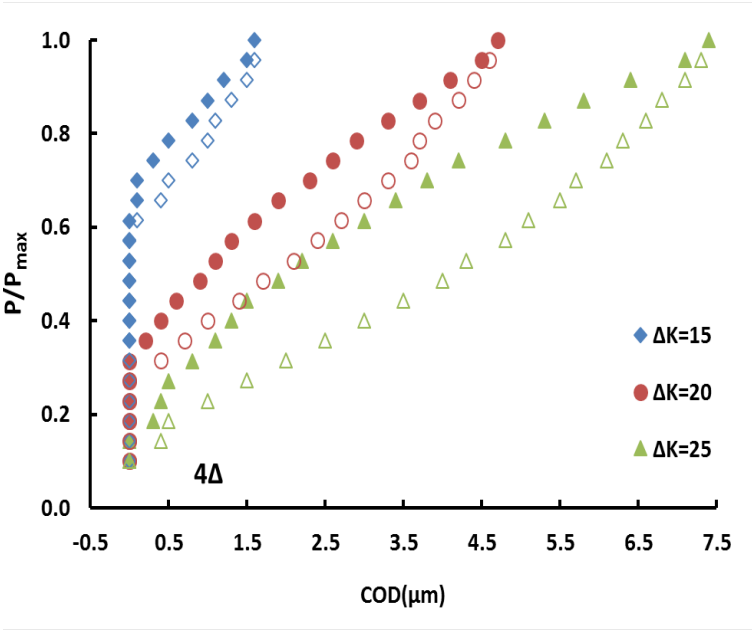

(c)

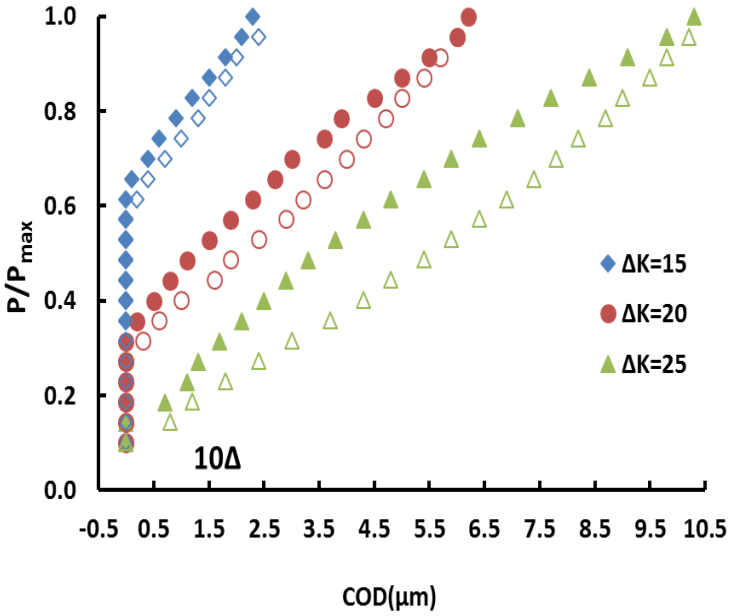

(d)

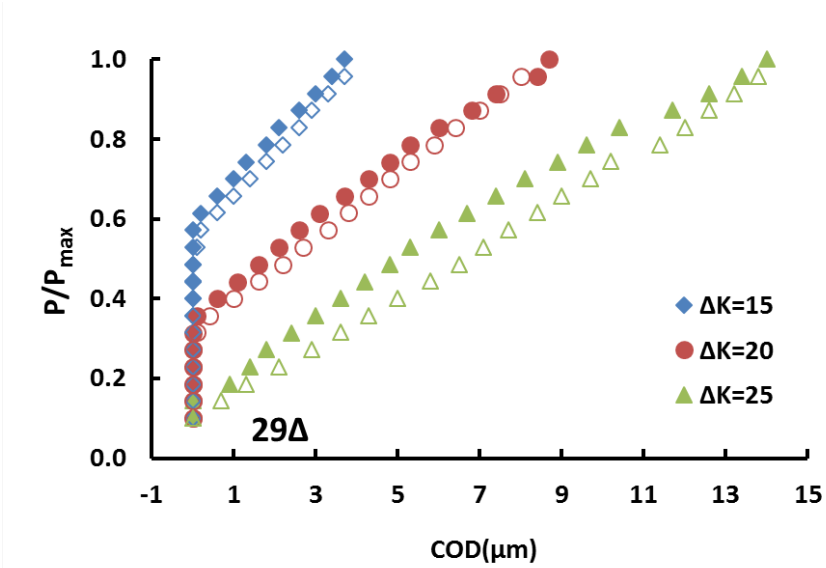

(e)

Figure 7. The development of COD during loading and unloading measured for the three load cases and at the selected distances to the crack tip (FOV_1).

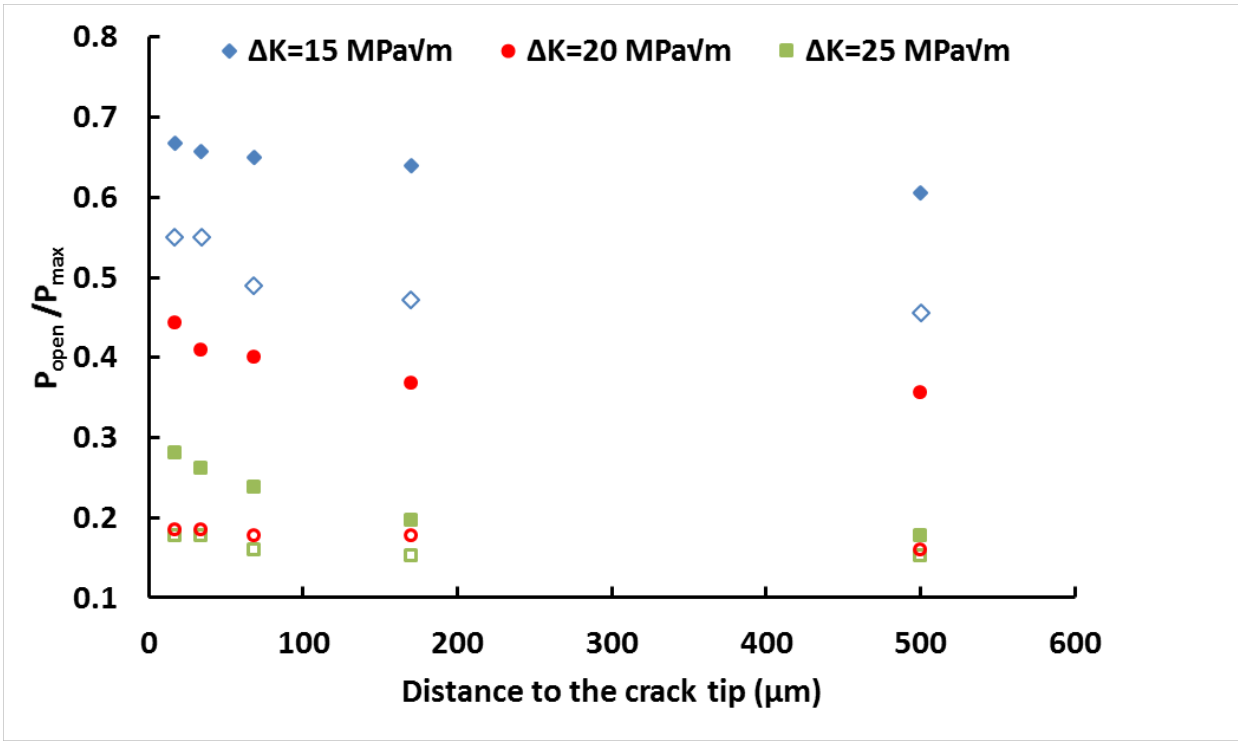

Figure 8. Crack opening loads as a function of distance to the crack tip, the effects of load level and the size of the field of view (FOV): (Closed - FOV_1; Open - FOV_2).

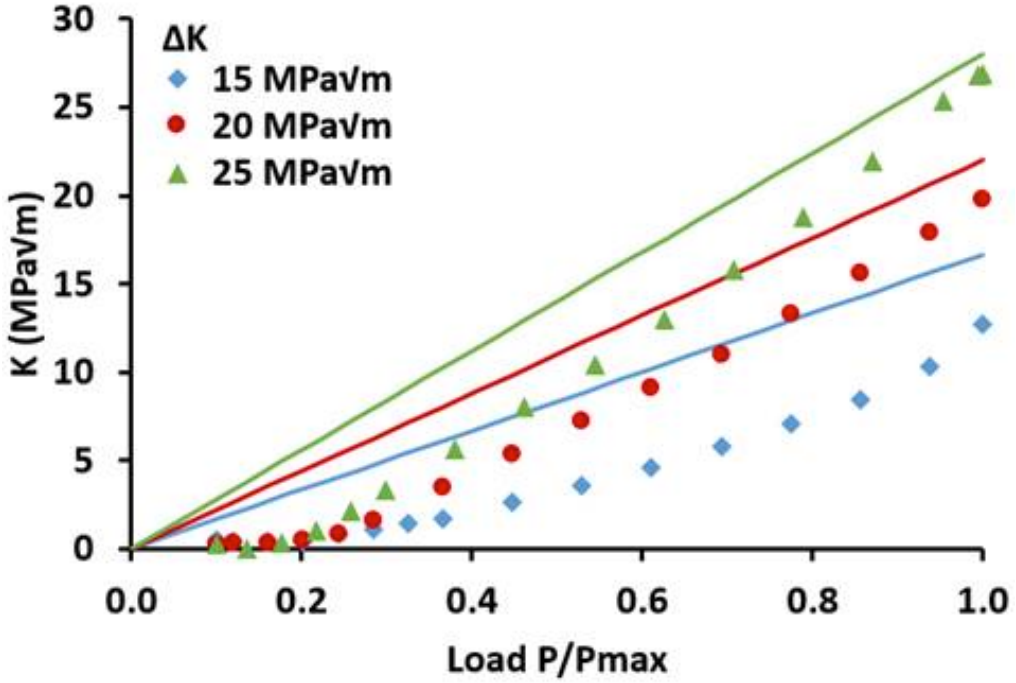

Figure 9. The stress intensity factors estimated from the full-field displacement data obtained from macro-DIC (FOV_2) as a function of applied load (symbols). The analytical solutions for a standard CT specimen are also included (lines).